JJMIE

Jordan Journal of Mechanical and Industrial Engineering

Design, Study, and Comparison of a New Axial Fan Using the Fibonacci Spiral and a Classic Axial Fan

Harry Aarón Yapu Maldonado

Coordinación de Investigación, Facultad de Ingeniería, Universidad Continental, Av. Los Incas s/n, Arequipa, Perú..

Abstract

This study aims to compare two small-sized axial fans: one is the classic axial fan (referred to as "Model A") and the other is an innovative design using the natural pattern of the Fibonacci spiral (referred to as "Model B"), which is found in natural phenomena such as hurricanes, nautilus shells, galaxies, and more. The comparison process is carried out using the Solidworks Flow Simulation tool, generating torque, flow, speed, noise level, and pressure graphs through parametric simulations.

The study arises from the growing need for efficient, quiet, and low-energy cooling to dissipate heat generated by electronic components. The methodology follows a logical and proprietary sequence, broken down into three design phases. In Phase 1, models are developed following the Fibonacci spiral constraint and simulated at 2000 RPM to maximize fluid flow. Phase 2 focuses on optimizing speed and flow by varying the angle of attack, the number of blades, and their length. Finally, Phase 3 presents the final model, with dimensions similar to the classic design but featuring stratified and curved blades, and a thickness of 0.5 mm to improve flow.

The most notable results reveal that the new design exhibits low levels of torque, flow, and noise. For example, at speeds greater than 3500 RPM, Model B shows an average noise reduction of 3.4%. Under the same torque consumption conditions, Model B rotates at 6000 RPM and Model A rotates at 3300 RPM; under these conditions, flow gains of up to 28.81% can be achieved. Under the same total pressure conditions, the maximum flow gain can reach 41%.

1. Introduction

In recent times, there has been a notable increase in the utilization of axial fans for cooling electronic components or heat transfer equipment[1],both in industrial and domestic settings [2],[3], which leads designers to make improvements to them to maximize their performance[4],[5], and reduce the noise they generate [6],[7]. Most of the research is based on improving existing axial fan designs[8], with a concentration on studies involving aerodynamic profile geometry or inlet geometry[9],[10], others study the effects of blade twisting or airfoil [11]–[14],and others studied the behavior of the fluid and its influence on fan noise generation[15],[16].

After analyzing different models and taking into account the trend observed in the literature, the present work proposes an innovative design of an axial fan based on Fibonacci spirals, reviewing inspiring ideas from previous work oriented to the design of vertical axis wind turbines [17]–[19].

The Fibonacci spirals are natural patterns found in fluid flow, evident in phenomena such as hurricanes, water vortices, galaxies, etc., as depicted in Figure 1. The proposed geometry in this study was analyzed through numerical simulation using Computational Fluid Dynamics (CFD)[20]–[24]. The objective of this study is to design a singular axial fan with optimal performance using Fibonacci spirals. The advantages presented by the proposed geometry have been numerically compared using Solidworks Flow Simulation, with the behavior of a classic axial fan serving as a reference. Experimental analysis was excluded from the scope due to technological limitations, but comparative parameters from four axial fan manufacturers were sought to enhance the reliability of numerical data.

2. Methodology

The designed methodology comprises three stages, as illustrated in Figure 2. Each of these stages addresses the solution of the Navier-Stokes equations for a stationary, isothermal, and incompressible flow. These calculations were carried out through numerical simulations using the Solidworks Flow Simulation tool.

The first phase of the design focused on the geometric application of the Fibonacci spiral as the primary constraint. Each design in this stage underwent simulations

---

at 2000 RPM, aiming to achieve the model with the maximum fluid particle velocity at this speed. To establish a benchmark in terms of maximum velocity, a comparison was made with the velocity values obtained from the classic model, also at 2000 RPM.

The second stage of the design process focuses on searching for an optimal design by varying the angle of attack and the number of blades. The primary goal is to consistently increase fluid velocities in the axial direction of the fan, thereby leading to an increase in its dynamic pressure. In this phase, the concept of using blades at multiple levels is implemented, as suggested[25],with the purpose of increasing the total air pressure. This approach aims to maximize the efficiency and performance of the overall system.

The third stage of the design process focuses on obtaining fundamental charts that illustrate the relationships between pressure, flow rate, acoustic power, and torque as a function of the fan's revolutions per minute (RPM). These charts provide a comprehensive and detailed insight into how these properties vary as the fan's RPM is adjusted. This comparative evaluation is essential for determining the performance and efficiency of the new design compared to Model A.

2.1. Design stage 1

As illustrated in Figure 3, seven representative models are presented, although a greater number has been developed in reality. The highlighted models are carefully detailed for better understanding. It is observed that all models have been shaped to comply with the restriction of adopting the Fibonacci pattern as a base. Additionally, an attempt was made to conceive a model without a core, and variations in the angles of attack in each design, along with the blade twist and variations in their number, are evident. This variability illustrates the diversity in exploring solutions during this initial design stage.

2.2. Design Stage 2

As illustrated in Figure 4, in this stage, the focus is on improving fluid velocity through the continuous variation of the angle of attack, the number of blades, and their length. The central purpose is to increase both the flow rate and dynamic pressure. This is achieved by strategically adding extra blades to fill the empty spaces between blades, compared to the previous stage. It is vital to maintain synchronization between the blades to avoid any disruption in the flow, thus preventing unwanted reversals in the velocity direction. This phase is oriented towards the ongoing optimization of the design to achieve higher performance.
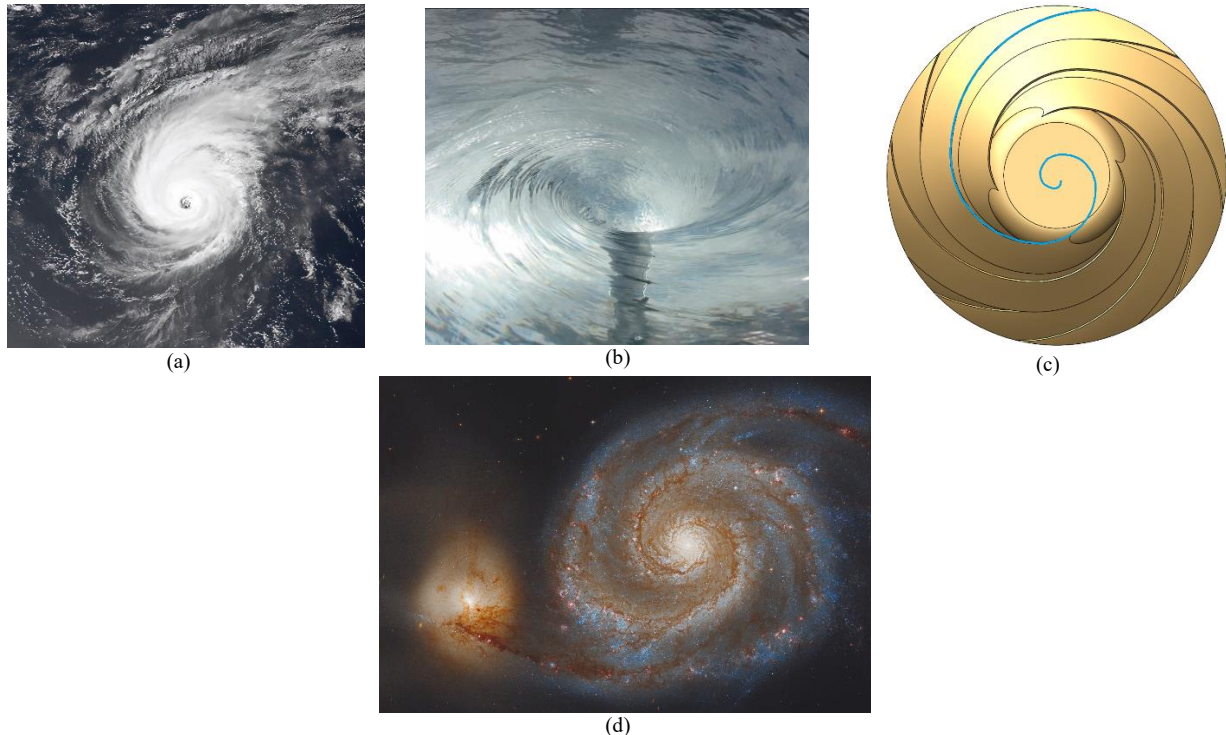

Figure 1. Natural Fibonacci patterns. (a) Photograph of a hurricane. (b) A whirlpool of water. (c) Model B developed. (d) M51 Whirlpool Galaxy
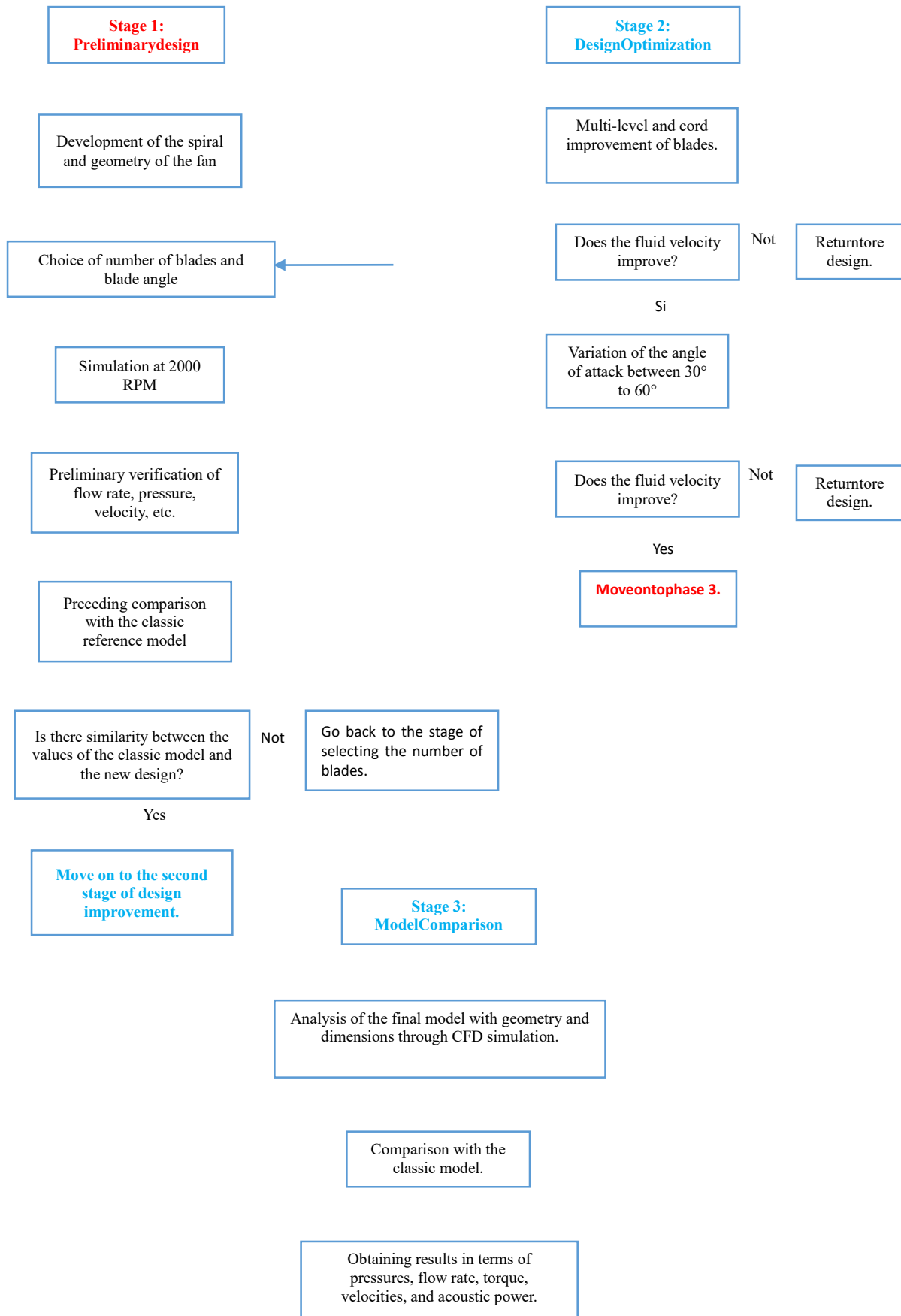
Stage 1:
Preliminarydesign

Development of the spiral
and geometry of the fan

Choice of number of blades and
blade angle

Simulation at 2000
RPM

Preliminary verification of
flow rate, pressure,
velocity, etc.

Preceding comparison
with the classic
reference model

Is there similarity between the
values of the classic model and
the new design?

Not → Go back to the stage of
selecting the number of
blades.

Yes

Move on to the second
stage of design
improvement.

Stage 2:
DesignOptimization

Multi-level and cord
improvement of blades.

Does the fluid velocity
improve? — Not → Returntore
design.

Si

Variation of the angle
of attack between 30°
to 60°

Does the fluid velocity
improve? — Not → Returntore
design.

Yes

Moveontophase 3.

Stage 3:
ModelComparison

Analysis of the final model with geometry and
dimensions through CFD simulation.

Comparison with the
classic model.

Obtaining results in terms of
pressures, flow rate, torque,
velocities, and acoustic power.

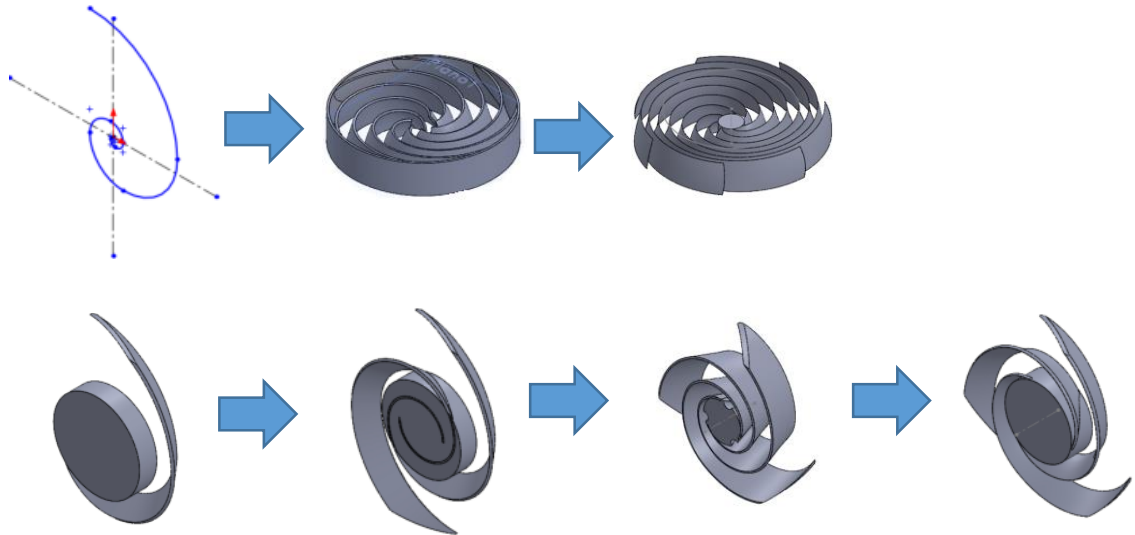**Figure 2.** Design stages for the new model

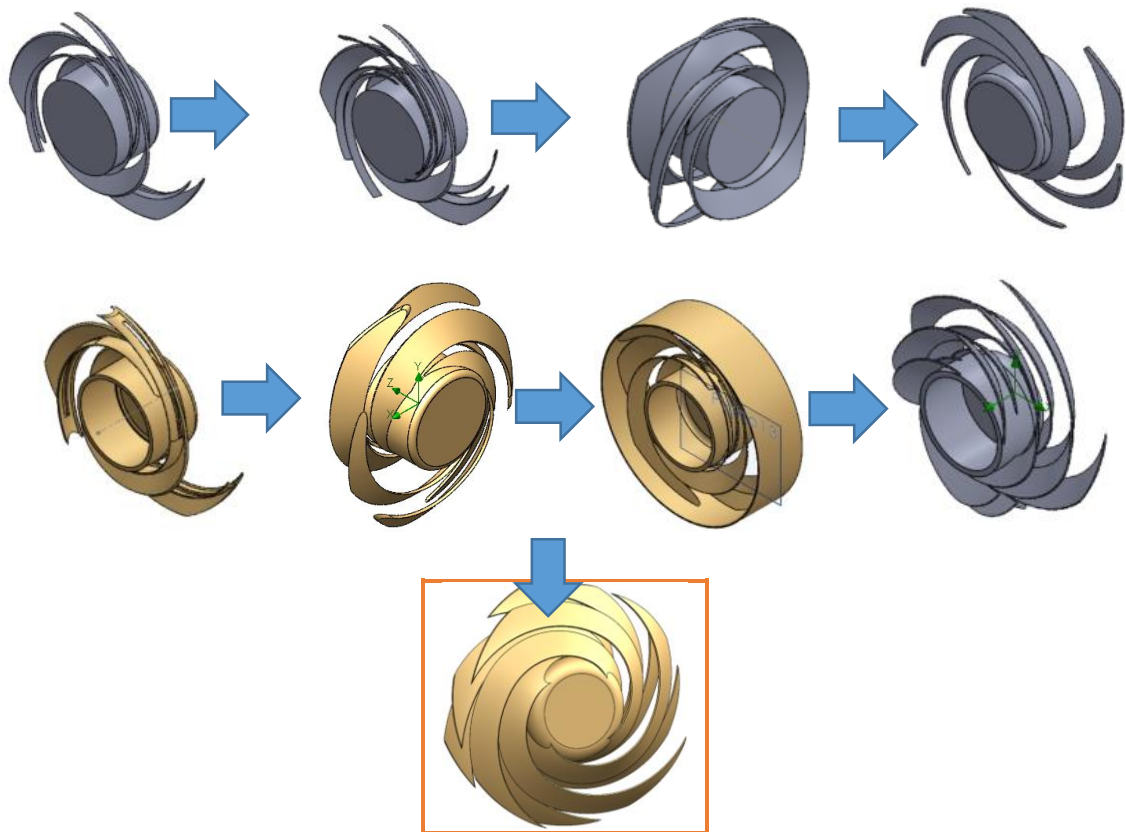**Figure 3.** Evolution of fan prototypes in the first stage of design

Figure 4. Evolution of fan models in the second stage. The fan in the orange box is the final model with the best performance.

2.3. Design Stage 3

In this culminating phase of the design process, we successfully obtain Model B, whose representation is depicted in Figure 5. This new design maintains dimensions similar to Model A, with an outer diameter of 80 mm and a blade width of 23 mm. It is important to note that this width is 1 mm greater than that of Model A; this variation was introduced to avoid welding the blades at each level and to ensure measurements did not exceed two decimal places, details that are visible in Figure 5.

Model B features three levels of stratified blades, each composed of four blades inclined at 45°. Although Figure 5 shows an inclination of 46°, this is due to a subtle curvature present in the blades. The blade thickness has been set at 0.5 mm to optimize the flow, following the guidelines of[4]and[6]. This final design is the result of a process of constant iteration and refinement, aimed at achieving superior performance and outstanding efficiency in the fan's operation.

3. Numerical results

3.1. Initial Conditions and Assumptions

Table 1 Initial conditions and assumptions

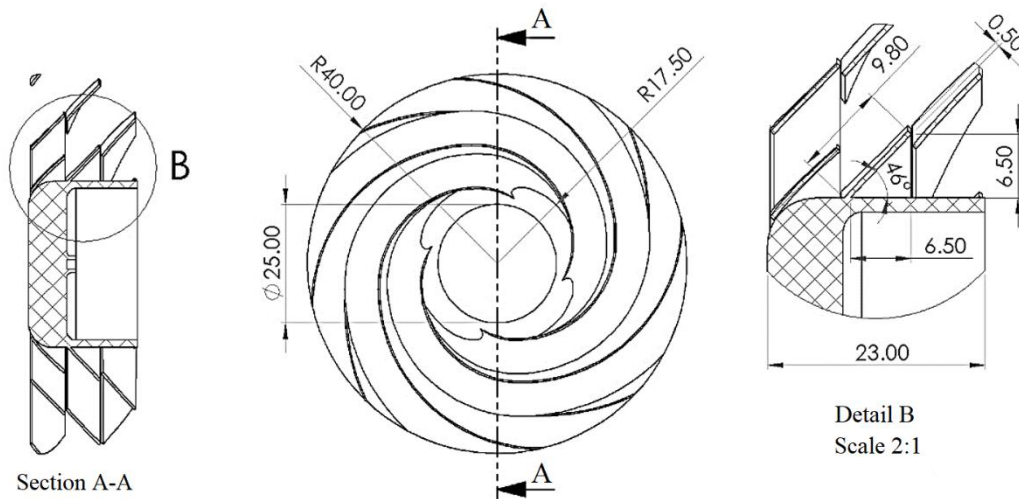| Initial conditions		Assumptions	
Atmospheric pressure	101325 Pa	Material:	General Purpose PBT
Density	1.2 kg/m3	Flow:	Stationary, incompressible, three-dimensional
Initial speed on all three axes	0 m/s	Viscosity Work:	Despicable

Figure 5. Final dimensions of model B.

The Navier-Stokes equations solved numerically are as follows:
Incompressible Flow Continuity Equation:

$$\frac{\partial u}{\partial x} + \frac{\partial v}{\partial y} + \frac{\partial w}{\partial z} = 0 \tag{1}$$

Component "x" of the Navier-Stokes equation of incompressible flow:

$$\rho\left(\frac{\partial u}{\partial t} + u\frac{\partial u}{\partial x} + v\frac{\partial u}{\partial y} + w\frac{\partial u}{\partial z}\right) = -\frac{\partial P}{\partial x} + \rho g_x + \mu\left(\frac{\partial^2 u}{\partial x^2} + \frac{\partial^2 u}{\partial y^2} + \frac{\partial^2 u}{\partial z^2}\right) \tag{2}$$

Component "y" of the Navier-Stokes equation of incompressible flow:

$$\rho\left(\frac{\partial v}{\partial t} + u\frac{\partial v}{\partial x} + v\frac{\partial v}{\partial y} + w\frac{\partial v}{\partial z}\right) = -\frac{\partial P}{\partial y} + \rho g_y + \mu\left(\frac{\partial^2 v}{\partial x^2} + \frac{\partial^2 v}{\partial y^2} + \frac{\partial^2 v}{\partial z^2}\right) \tag{3}$$

Component "z" of the Navier-Stokes equation of incompressible flow:

$$\rho\left(\frac{\partial w}{\partial t} + u\frac{\partial w}{\partial x} + v\frac{\partial w}{\partial y} + w\frac{\partial w}{\partial z}\right) = -\frac{\partial P}{\partial z} + \rho g_z + \mu\left(\frac{\partial^2 w}{\partial x^2} + \frac{\partial^2 w}{\partial y^2} + \frac{\partial^2 w}{\partial z^2}\right) \tag{4}$$

3.2. Sensitivity Study of the Mesh

To ensure the reliability of the results, a mesh independence study was conducted. This study was carried out at 2000 RPM for both models, and the results are detailed in Table 2 and Table 3. In the case of Table 2, mesh level 5 was chosen as the selected level because the velocity stabilizes at 0.037 m/s following the criteria of M. Maine *et al*[26]y M. Hadipour *et al*[14], [27]. Mesh level 3 could have been chosen, with a velocity of 0.0385 m/s, but the percentage difference between levels 3 and 5 is 4.04%, making level 5 the better option. Another option could have been to mesh using commercial software like GAMBIT, as done by Y. Taamneh *et al*[28].

In the case of Table 3, mesh level 5 is selected because the velocity stabilizes at 0.0072 m/s, and there is a difference of 6.63%, which represents the lowest value. Level 4 could have been chosen, but it has a very high velocity value. Therefore, level 5 provides an intermediate value between levels 3 and 4, and additionally, the percentage difference between levels 3 and 5 is only -5.15%.

For the reasons already explained, simulations were carried out for both models using mesh level 5.

3.3. Calculations CFD

3.3.1. Preprocessor

The computational domain: It has dimensions of length, width, and height= $200 \times 100 \times 100$ mm

Mesh level in both models: Level 5

The boundary conditions are: Real wall for all surfaces, both rotor and stator, with a roughness of 3.2 micrometers.

3.3.2. Solver:

SolidWorks solves the continuity equations and the equation of motion.

3.3.3. Post-processor

At this stage, you can visualize the representation of the two models under analysis. Figure 6 shows Model A in red and Model B in gold. Both models use the same stator, enabling a more direct comparison of their features and performance. With these details, the framework is established for the results analysis, where information about air flow, pressure, velocity, and other key parameters is expected. This will allow a comparison between the two models and an evaluation of how the redesign based on the Fibonacci spiral has influenced the fan's performance.

Table 2. Model A - Mesh Sensitivity

Mesh level	No. of Elements	Axial velocity (m/s)	Reynolds Number (Re)	Difference (Re)
1	14 590	0.0118	64.56	-0.73%
2	27 777	0.0119	65.03	-222.56%
3	65 971	0.0385	209.76	22.09%
4	130 489	0.03	163.42	-23.16%
5	245 876	0.037	201.27	-4628.10%
6	415 268	1.936	9516.25	--

Table 3. Model B - Mesh Sensitivity

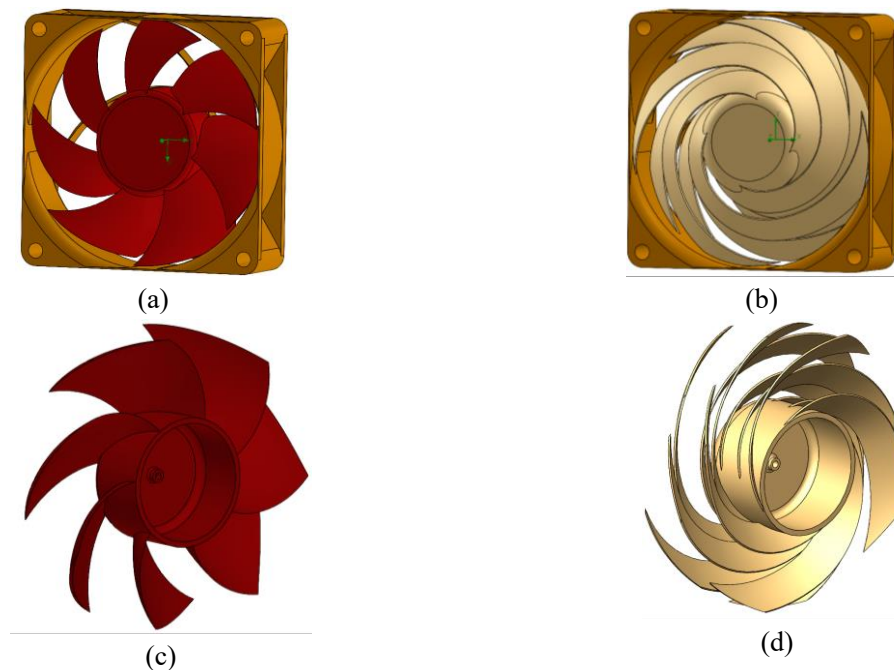| Mesh level	No. of Elements	Axial velocity (m/s)	Reynolds Number (Re)	Difference (Re)
1	18 886	0.0027	14.74	-68.67%
2	24 971	0.0046	24.87	-49.05%
3	70 268	0.0068	37.07	12.63%
4	118 108	0.0077	41.75	6.63%
5	275 945	0.0072	38.98	41.47%
6	853 408	0.0042	22.81	--

(a)

(b)

(c)

(d)

Figure 6. Simulated models with their stator and rear view of the rotor. (a) Model A. (b) Model B. (c) Rear view of Model A. (d) Rear view of Model B.

In Figure 7, the simulation results at 2000 RPM are presented, showing the trajectory lines for the models in Figure 7(a) and 7(b). Specifically, the average outlet velocities are recorded as 3.43 m/s for Model A and 2.67 m/s for Model B. This finding highlights how the redesign based on the Fibonacci spiral has influenced the air flow velocities, with a reduction in Model B.

Figures 7(c) and 7(d) show the pressure distribution on the surfaces of the models. It is evident that Model A exhibits a higher-pressure increase, with a value of 101341.06 Pa at the outlet, compared to Model B, which records 101326 Pa. This difference may influence the overall performance and efficiency of the system.

Regarding noise, Figures 7(e) and 7(f) show that both models do not disperse noise beyond the control volume. However, Model B exhibits areas of higher noise concentration within the rotor. This may be attributed to the greater number of blades in the design, which will be examined in detail in the results section.

In general, these results highlight how the redesign based on the Fibonacci spiral has generated differences in velocities, pressures, and noise distribution compared to the classical design. These data provide a basis for evaluating how the new design exhibits its own behavior.
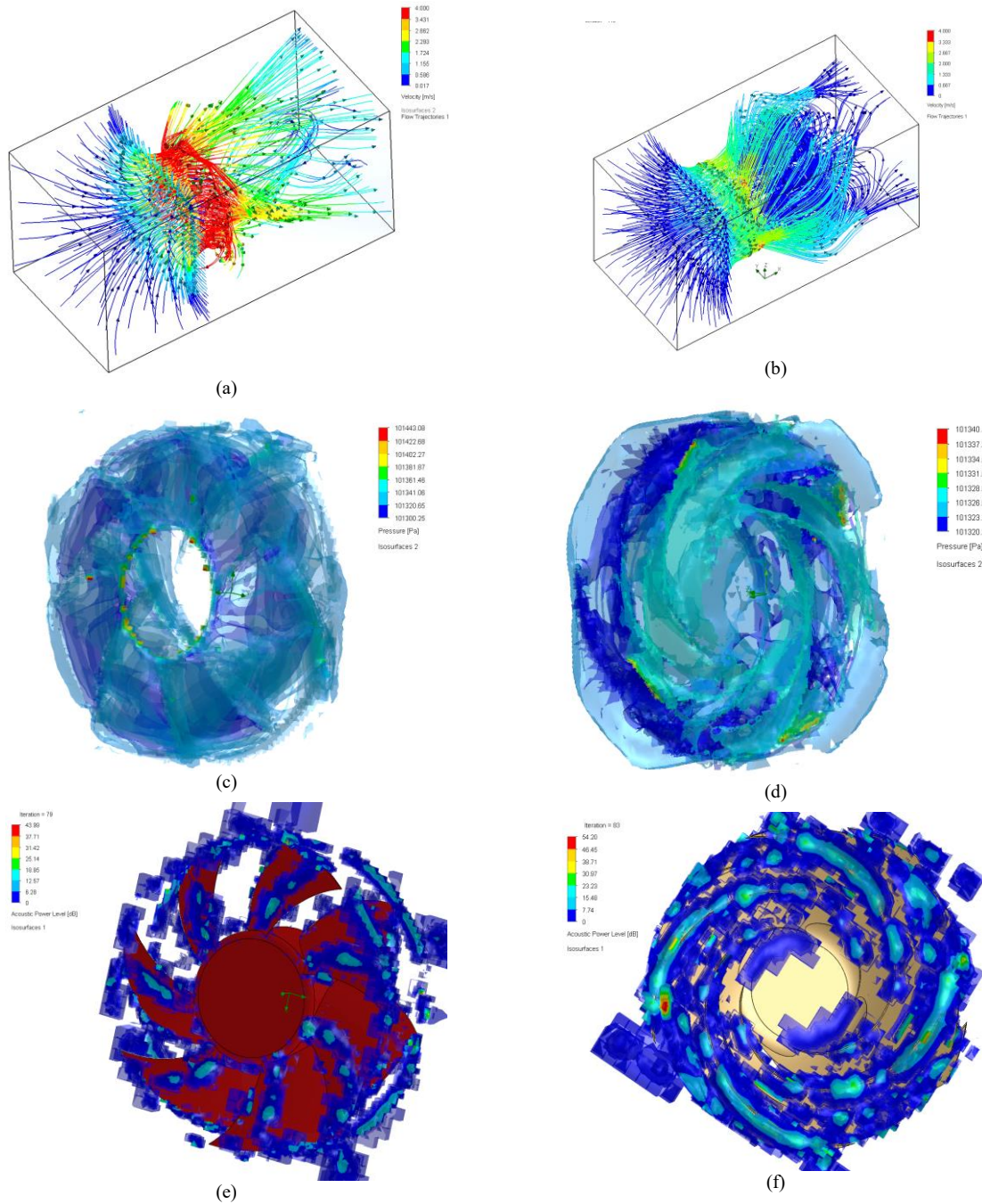

Figure 7. Results of the second stage for Model A: (a) Trajectory lines at 2000 RPM for Model A, (b) Trajectory lines at 2000 RPM for Model B, (c) Cut view of the pressure field at 2000 RPM for Model A, (d) Cut view of the pressure field at 2000 RPM for Model B, (e) Isosurface of acoustic power at 2000 RPM for Model A, (f) Isosurface of acoustic power at 2000 RPM for Model B.

The provided description regarding the acquisition of performance curves is valuable for understanding the process and methodology used:

To generate the performance curves for the two fan models, a virtual test bench was created simulating a duct with different outlet diameters (0 mm, 27 mm, 42 mm, 57 mm, 72 mm). This virtual test bench provides the scenario in which the performances of both fans are evaluated and compared.

The fan models underwent a parametric study using a mesh refinement level of Level 5. Additionally, three parametric simulations were conducted for each configuration to obtain reliable average values. This ensures that the results are representative and consistent.

Figure 8 provides a visualization of this process and how parametric simulations were organized to obtain performance curves. This methodological approach provides a solid understanding of how the performance curves for both models were generated and evaluated, enabling an objective comparison of their performance under different conditions and outlet diameters.

The information provided about the comparison and the refinement level selection process is important to support the reliability of the results:

To ensure the adequacy of the refinement values and mesh level, a comprehensive comparison of the characteristics of different fans with dimensions similar to the classical model of $80 \times 80 \times 20 \pm 5$ mm, was carried out, as done by [29]-[30]. The evaluated characteristics include respective acoustic powers, flow rates, and static pressures.

Results of this comparison are summarized in Table 4, providing reference values for the selection of mesh refinement level, as experimental measurement is not feasible. It is observed that pressure values range between 13 and 22 Pascals, flow rates fluctuate between 27 and 50 m^3/h, and noise levels vary between 16 and 26 dBA.

This comparison is crucial to ensure that the selected refinement level is appropriate and capable of accurately capturing the flow characteristics and performance of the fan models under analysis. The results obtained through this methodology should be more reliable and relevant in terms of their real-world application.
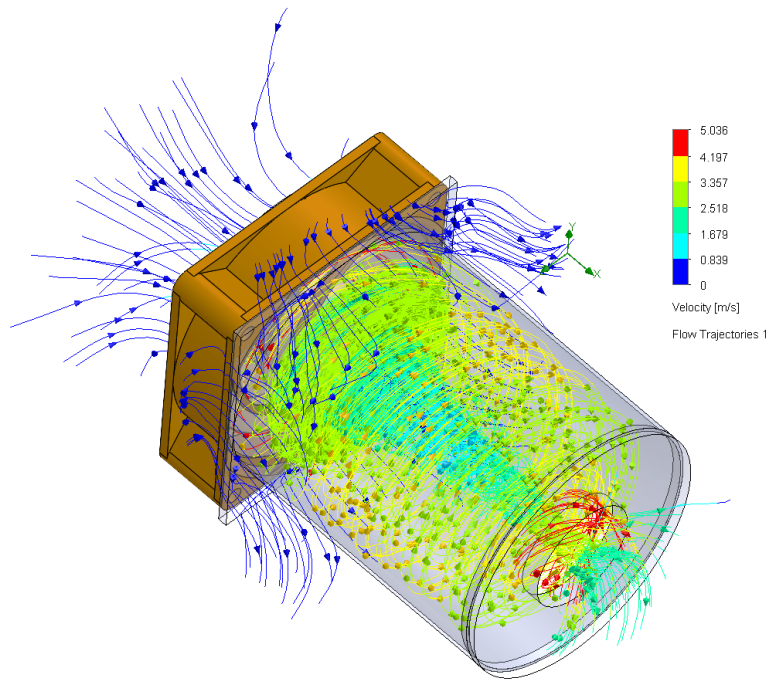

Figure 8. Test bench results for Model B at 3000 RPM.

Table 4. Reference models to validate simulation results for Model A.

Model	Material	Dimensions (mm)	RPM	Static Pressure (Pa)	Flow (m³/h)	Noise level (dBA)	Ref.
CASE FAN 12 VDC	PBT	80×80×20	2500	19.22	49.57	26	[29]
NF-A8 FLX	PBT	80×80×25	2000	19.22	50.4	16.1	[31]
XYJ12B8020L	Thermoplastic	80×80×20	2000	13.53	27.59	24.5	[32]
DC FAN	-	80×80×20	2400	22.40	46.61	25	[30]

4. Results and discussions

In Figure 9(a), it can be observed how static pressure behaves according to expectations for this type of fans. As the flow rate increases, static pressure tends to decrease, following a predictable pattern. It's worth mentioning that the curves corresponding to Model A show a concave shape, while the curves of Model B adopt a convex shape. This observation is key to understanding the differences in the behavior of the two models.
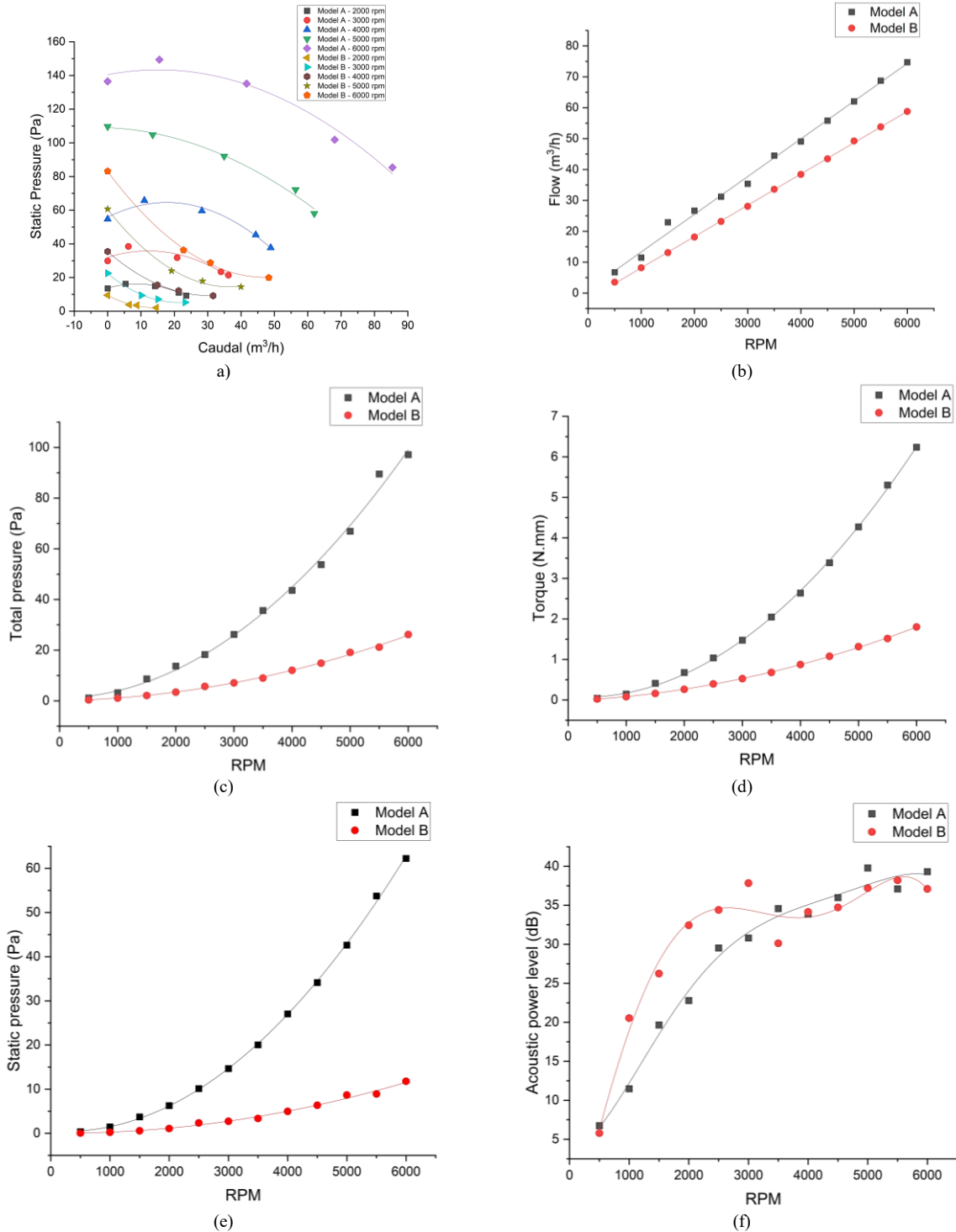
Figure 9(a) compiles simulations conducted starting from 2000 RPM, with intervals of 1000 RPM between them. This interval choice originates from the design criterion established in phase 1 of the study. The goal was to avoid saturating the graphs with too many data points to ensure a clear and understandable visualization of the relationship between static pressure and flow rate in different speed configurations.

Figure 9. Results of parametric simulations from 500 to 6000 RPM with intervals of 500 RPM. (a) Static pressure vs RPM. (b) Flow rate vs RPM. (c) Total pressure vs RPM. (d) Torque vs RPM. (e) Static pressure vs Flow rate. (f) Acoustic power vs RPM.

(a)   (b)
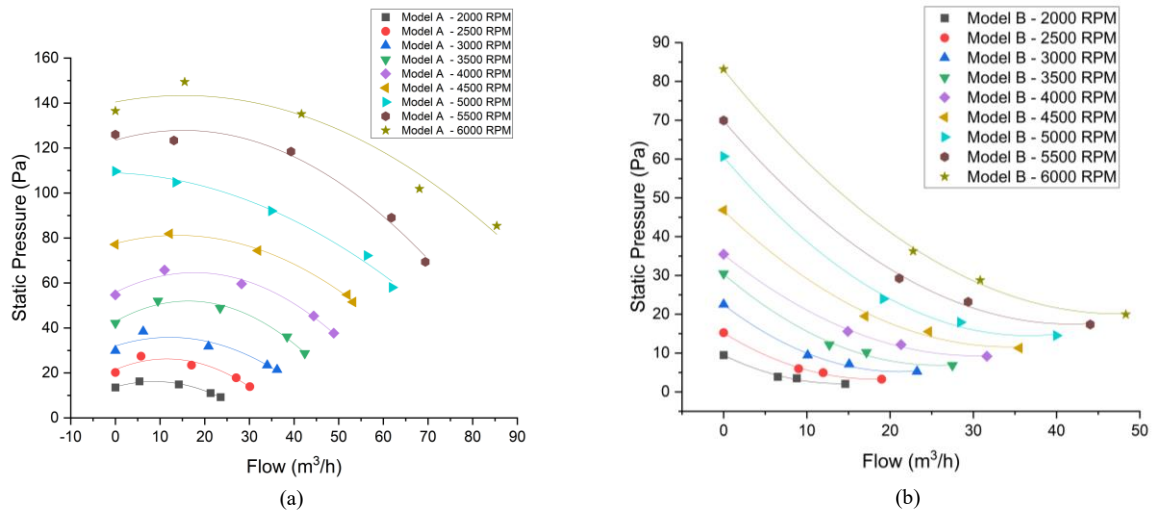
Figure 10. Variation of static pressure and flow rate from 2000 RPM to 6000 RPM. (a) Model A, (b) Model B.

In Figure 9(b), it is observed that Model A (black line) achieves a higher flow rate compared to Model B (red line), especially at 6000 RPM, where the difference is 21.32% in favor of Model A. At 3000 RPM, the gap between the models is 20.58%. This is due to the increased number of blades and also the surface area, thanks to the Fibonacci spiral geometry.

Figure 9(c) reveals that the total pressure is higher in Model A (black line) compared to Model B (red line). The percentage difference reaches 73.07% at 6000 RPM. This disparity is due to the greater contribution of static pressure in Model A, resulting in a steeper growth of the total pressure curve.

In Figure 9(d), it can be seen that the torque of Model A (black line) exceeds that of Model B (red line) by 71.09% at 6000 RPM. Additionally, the graph shows that the torque increase of Model A follows a parabolic trend with a smaller opening as revolutions increase, while in Model B, the curve is also parabolic but with a larger opening.

In Figure 9(e), when analyzing the relationship between static pressure and RPM, it is evident that the maximum pressure in Model A (represented by the black line) exceeds that recorded in Model B (represented by the red line) by 81.07% at 6000 RPM. This phenomenon was expected as observed by Hirano *et al*[4]because Model B has a shorter chord length (9.8 mm) than Model A (32 mm), which clearly explains why Model B exhibits lower static pressure values.

In Figure 9(f), the level of acoustic power, representing the average of values in each of the different regions of the control volume, as illustrated in Figures 7(e) and 7(f), is observed. In all cases, three simulations were conducted, and the average of these simulations was calculated. It is relevant to note that, from 3500 RPM onwards, the acoustic power of Model B decreases and remains below the acoustic power of Model A. Quantifying the reduction, at 4000 RPM, the reduction is 6.08%, at 4500 RPM it is 4.6%, at 5000 RPM it is 1.33%, at 5500 RPM it is 0.8%, and finally, at 6000 RPM, it is 4.18%. The advantages of Flow Simulation for noise prediction[33], lie in its use of a Fast Fourier Transform (FFT) algorithm that predicts noise from an

isotropic volume of turbulence and does not require transient data.

When observing the overall behavior of model B in Figure 9, it can be deduced that the Fibonacci spiral allows an increase in the surface area and the number of blades that enhance the flow, albeit to a lesser extent than model A. A lower torque consumption in model B confirms that the drag force is reduced, thus allowing a better transfer of kinetic momentum without causing excessive exit vortices. On the other hand, model B clearly does not increase static pressure, owing to the shape and narrower width of the blade. Consequently, the pressure waves upon leaving the rotor are not entirely longitudinal but rather helical in form, as confirmed by Figure 7 (d). Additionally, the expansion volume for the pressure waves is reduced due to the stratified arrangement of the blades.

In Figure 10, the behavior of static pressure and flow rate for the virtual test bench is shown, which was used to obtain the fan curves. It is important to note that the curve corresponding to Model A shows a concave behavior, while the curve of Model B exhibits a convex shape. In Figure 10(b), the graphs were obtained using only four caps at the outlet (0 mm, 42 mm, 57 mm, 72 mm). This choice is due to the fact that, for the 27 mm cap, Model B is choked and does not yield logical values for the flow rate. This situation results in a highly scattered polynomial regression of the simulation data and, therefore, alters the integrity of the polynomial regression.

In Figure 11, it is observed that Model A has a higher Reynolds number compared to Model B, indicating that Model A accelerates fluid particles more than Model B. Therefore, the kinetic momentum in the axial direction is greater for Model A.

Figure 12 shows the presence of vortices in each model. Figure 12(a) corresponds to Model A, and it can be seen that the number of vortices within the rotor in a steady state has a larger surface area of propagation (maximum value of 1387.01 s^{-1}) than Model B (Figure 12(b)), with its maximum value being 2704.99 s^{-1}. Note that regions of high vorticity develop from the middle radius to the outer radius of the impeller for Model A,

while in Model B, they only concentrate on the outer radius and coincide with the blade tips, with lower values. In Figures 12(c) and 12(d), the same trend is observed; Model A has larger regions of high vorticity at 6000 RPM compared to Model B. These results could be explained by what was observed by J. O. Mo *et al*[15],where flow separation on the blades affects performance and increases noise. It would also support this explanation reported by Yang *et al*[11], who found that the noise level increases due to blade twist when they have a positive angle. However, this would only explain the high noise at speeds below 3500 RPM for Model B, as the shape of the blades has a greater twist angle than Model A. Based on the results in Figure 12, we can deduce that Model B, at speeds above 3500 RPM, forces the fluid to adopt a more laminar flow following the Fibonacci pattern. With higher RPM, the fluid has more kinetic energy, channeled by the rotor's geometry, which reduces fluid detachment from the blade (also having a smaller chord value) and therefore generates fewer vortices[34]. We must also add that we followed the recommendation of Ito, *et al*[7], by placing the smallest separation value between the rotor and stator (0.5 mm) and the negative radius angle (in both models) to minimize the influence of this generated noise.
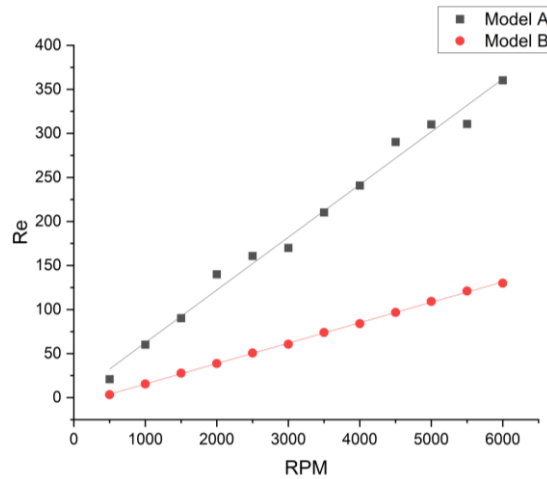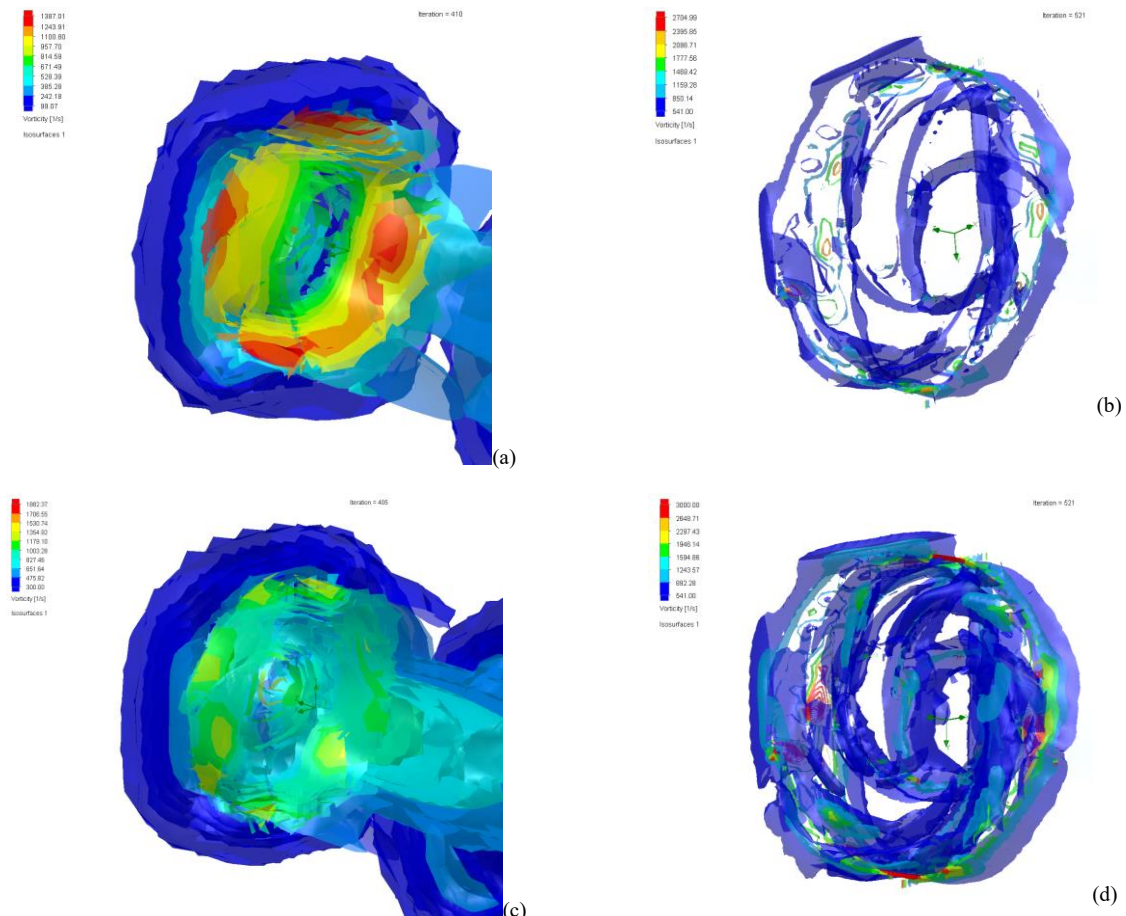

Figure 11. RPM vs Reynolds Number (Re)

(a)

(b)

(c)

(d)

Figure 12. Vorticity iso-surface (a) Model A at 3500 RPM, (b) Model B at 3500 RPM, (c) Model A at 6000 RPM, (d) Model B at 6000 RPM

5. Conclusion

We can conclude the reliability of the simulation data due to the choice of similar models, such as the cases of CASE FAN 12 VDC and XYJ12B8020L from Table 1. When comparing the acoustic power values for speeds of 2000 and 2500 RPM, a notable correspondence is observed between the simulation results and the values recorded in Table 1. For example, the regression curve shows values of 24.06 dBA and 28.44 dBA, respectively, while Table 1 reports 26 dBA and 24.5 dBA for the same speeds. Regarding the static pressure and flow rate of the CASE FAN 12 VDC model at 2000 RPM, the values obtained from the regression curve (23.57 m^3/h and 9.09 Pa) are compared with the values from Table 1 (49.57 m^3/h and 19.22 Pa). For the XYJ12B8020L model at 2500 RPM, the results from the regression curve (27.59 m^3/h y 13.53 Pa) align with the values from Table 1 (30.09 m^3/h and 13.75 Pa). In contrast, the NF-A8 FLX and DC FAN models exhibit notable differences in terms of pressure and flow. The Noctua NF-A8 FLX has a greater geometric width (25 mm), despite having the same number of blades. It is important to note that this is due to the absence of experimental simulation data, and we aim to have more certainty about the numerical results. With regard to the fan material, it is important to study the roughness, as it has significant effects on the drag coefficient according to H. Moria et al [35], although it was not the subject of the study, it is inherently included because the data from Table 1 and the numerical simulation were taken into account to extract the comparison parameters for this study. In the case of the DC FAN, the lack of data on the number of blades and the material complicates direct comparison. However, it is observed that the noise level values in the regression calculations approximate the values obtained in practice. Overall, these results support the reliability of the simulation data, as they show consistency with previously analyzed and validated models, reinforcing the robustness of the data obtained in this study.

It can be concluded that model B offers an average reduction in noise of 3.4% from speeds higher than 3500 RPM. This is due to the fact that this geometry forces the fluid to adopt laminar flow, has less drag resistance, which is attributed to the geometry of the blades having a smaller chord length, and generates fewer exit vortices. This reduction in noise level is beneficial, as in axial fans, sound tends to increase with the increase in RPM.

It is concluded that model B will have lower energy consumption due to lower resistance to rotation. This is evident because the torque multiplied by the RPM provides the value of the mechanical power required to overcome air resistance. For example, if we focus on a point where the acoustic powers are the same (Figure 9(f)) at 3500 RPM, the torque data for model A is 2.042 N.mm and for model B it is 0.6925 N.mm, resulting in a torque reduction in favor of the new model by 66.087%. However, it is important to consider that requiring less mechanical energy to drive the rotor will result in a reduction in flow rate, as observed in Figure 9(b). At 3500 RPM, the classical model can move 43.823 m3/h, while the new model reaches 33.5 m^3/h, representing a disadvantage of a 23.56% reduction in flow rate. If the model B were operated at 6000 RPM, and we look at

Figure 9(d), both models would have the same torque value of 1.8 N.m, only that the RPM for model A would be 3300 RPM. Taking these RPM values for model A and model B to Figure 9(b), the flow rate gain would be 28.81%. Consequently, there would be a greater gain in flow rate at speeds higher than 3300 RPM for model B compared to model A.

Some other advantages of model B over model A can be concluded from the torque and RPM graph in Figure 9(d). For example, if we select a torque of 1 N.mm for both models, from the regression, we obtain 2487.5 RPM for model A and 4320.8 RPM for model B. At these speeds, a maximum static pressure of 25.95 Pa is obtained for model A according to Figure 10(a), and for this same pressure, a flow rate of 11.5 m^3/h. is achieved. In the case of model B, starting from a pressure of 25.95 Pa and 4320.8 RPM, a flow rate of 12.3 m^3/h is obtained. Analyzing the noise level in Figure 9(f), a value of 28.35 dBA is obtained for model A and 34.02 dBA for model B. Therefore, if we quantify the benefit for the flow rate, a gain of 6.5% is obtained at the expense of an increase in the noise level of 16.67%. All of this is achieved while maintaining the same torque consumption and static pressure.

Similarly, to the previous analysis, it can be concluded that for the same total pressure of 21.93 Pa according to Figure 9(c), the following values are obtained for model A: 2752.7 RPM from Figure 9(c), 1.2415 N.mm from Figure 9(d), 30.15 dBA from Figure 9(f), and 34.7 m^3/h from Figure 9(b). As for the new model, starting from the same total pressure of 21.93 Pa according to Figure 9(c), the following values are obtained: 5500 RPM from Figure 9(c), 1.538 N.mm from Figure 9(d), 38.57 dBA from Figure 9(f), and 58.82 m^3/h from Figure 9(b). Therefore, if we quantify the benefit for the flow rate, we obtain a gain of 41%, but at the expense of an increase in noise level by 21.83% and torque by 19.28%.

Finally, it is concluded that Model B is less efficient in many of the parameters measured in this study. However, this does not rule out the possibility of leveraging its advantages under specific working conditions, where it outperforms Model A. Furthermore, it is noted that this study lacks experimental measurements and mathematical models that can directly predict the fluid's behavior and its relationship with the Fibonacci spiral. It is essential to emphasize that experimental results will allow us to accept or refute the numerical findings in a more objective manner.

Bibliography

[1] 雅一石川, 優介大槻, and M. Ishikawa Yusuke Otsuki 要旨, "Efficiency Improvement of Motor Fan for Cooling Radiator," pp. 32–38.

[2] M. Srivastava, P. Bishnoi, and M. K. Sinha, "Cfd Analysis of Cpu for Cooling of Desktop Computers", International Journal of Advanced Technology in Engineering and Science, Vol. 4, No. 08, 2016, pp. 693–700, [Online]. Available: www.ijates.com

[3] J. Jalil, E. Ali, and H. Kurdi, "Numerical and Experimental Study of Cooling in Desktop Computer with Block Heat Sink", Engineering and Technology Journal, Vol. 36, No. 4A, 2018, pp. 430–438, doi: 10.30684/etj.36.4a.10.

[4] T. Hirano, K. Takahashi, and G. Minorikawa, "Study on Performance Evaluation of Small Axial Fan", Open Journal of Fluid Dynamics, Vol. 07, No. 04, 2017, pp. 546–556, doi: 10.4236/ojfd.2017.74037.

[5] H.-H. Lin and J.-H. Cheng, "Computer Axial Flow Fan Optimization Design", KnE Social Sciences, Vol. 3, No. 10, 2018, pp. 1630–1639, doi: 10.18502/kss.v3i10.3498.

[6] G. Li, L. Zhu, Y. Hu, Y. Jin, T. Setoguchi, and H. D. Kim, "Influence of chord lengths of splitter blades on performance of small axial flow fan", Open Mechanical Engineering Journal, Vol. 9, No. 1, 2015, pp. 361–370, doi: 10.2174/1874155X01509010361.

[7] T. Ito, G. Minorikawa, A. Nagamatsu, and S. Suzuki, "Experimental Research for Performance and Noise of Small Axial Flow Fan", Journal of Environmental Engineering, Vol. 3, No. 1, 2008, pp. 192–203, doi: 10.1299/jee.3.192.

[8] R. Vijayakumar, D. Balamurugan, K. Hariharan, and K. Nithishrajan, "Design and Analysis of CPU Cooling Fan Blades Using Solidworks",Annals of the Romanian Society for Cell Biology, Vol. 25, No. 5, 2021, pp. 2077–2082.

[9] P. Liu, N. Shiomi, Y. Kinoue, Y. Z. Jin, and T. Setoguchi, "Effect of inlet geometry on fan performance and flow field in a half-ducted propeller fan", International Journal of Rotating Machinery, Vol. 2012, 2012, doi: 10.1155/2012/463585.

[10] S. A. Beskales, Samir S. Ayad, M. G. Higazy,O. Abdellatif,S. Anwar, "The Effect Of Tip End-Blade Geometry On The Axial Fans Performance", Eleventh International Conference of Fluid Dynamics, Alexandria, Egypt, 2013, doi: 10.13140/2.1.5047.1208.

[11] A. Yang, T. Tang, H. Zhang, and K. Chen, "Effect of Swept Blade on Performance of a Small Size Axial Fan", Fluid Machinery and Fluid Mechanics, No. 4, 2009, pp. 279–284, doi: 10.1007/978-3-540-89749-1_42.

[12] A. Zarri, J. Christophe, S. Moreau, and C. Schram, "Influence of Swept Blades on Low-Order Acoustic Prediction for Axial Fans",Acoustics, Vol. 2, No. 4, 2020, pp. 812–832, doi: 10.3390/acoustics2040046.

[13] D. Ghodake, M. Sanjosé, S. Moreau, and M. Henner, "Effect of Sweep on Axial Fan Noise Sources Using the Lattice Boltzmann Method", International Journal of Turbomachinery Propulsion and Power, Vol. 7, No. 4, 2022, pp. 34, doi: 10.3390/IJTPP7040034.

[14] M. Hadipour and E. Goshtasbi Rad, "Investigation of sweep angle effects on a submarine hydrodynamic drag using computational fluid dynamics," Jordan Journal of Mechanical and Industrial Engineering, Vol. 9, No. 3, 2015, pp. 209–216.

[15] J. O. Mo and J. H. Choi, "Numerical investigation of unsteady flow and aerodynamic noise characteristics of an automotive axial cooling fan", Applied Sciences, Vol. 10, No. 16, 2020, doi: 10.3390/APP10165432.

[16] X. Niu, "Numericaland experimental study on rotor-stator interaction noise of an axialfan", Acta AerodynamicaSinica, Vol. 39, No. 5, pp. 1-9, 2021, doi: 10.7638/kqdlxxb-415.

[17] J. Blanco, J. de D. Rodriguez, A. Couce, and M. I. Lamas, "Proposal of a nature-inspired shape for a vertical axis wind turbine and comparison of its performance with a semicircular blade profile", Applied Sciences, Vol. 11, No. 13, 2021, doi: 10.3390/app11136198.

[18] J. Blanco Damota, J. de D. Rodríguez García, A. Couce Casanova, J. Telmo Miranda, C. G. Caccia, and M. I. L. Galdo, "Optimization of a Nature-Inspired Shape for a Vertical Axis Wind Turbine through a Numerical Model and an Artificial Neural Network", Applied Sciences, Vol. 12, No. 16, 2022, doi: 10.3390/app12168037.

[19] "US9328717B1 - Golden ratio axial flow apparatus - Google Patents." https://patents.google.com/patent/US9328717B1/en (accessed Jan. 08, 2024).

[20] L. Wenguang, "Inverse Design of Impeller Blade of Centrifugal Pump with a Singularity Method", Jordan Journal of Mechanical and Industrial Engineering, Vol. 5, No. 2, 2011, pp. 119–128.

[21] I. Mabrouki, Z. Driss, and M. S. Abid, "Numerical study of the hydrodynamic structure of a water savonius rotor in a test section", Jordan Journal of Mechanical and Industrial Engineering, Vol. 8, No. 3, 2014, pp. 127–136.

[22] M. Saraireh, "Computational fluid dynamics simulation of plate fin and circular pin fin heat sinks", Jordan Journal of Mechanical and Industrial Engineering, Vol. 10, No. 2, 2016, pp. 99–104.

[23] A. V. Kolhe, R. E. Shelke, and S. S. Khandare, "Combustion modeling with CFD in direct injection CI engine fuelled with biodiesel", Jordan Journal of Mechanical and Industrial Engineering, Vol. 9, No. 1, 2015, pp. 61–66.

[24] C. Ghenai, T. Salameh, and I. Janajreh, "Modeling and simulation of shrouded Horizontal Axis Wind Turbine using RANS method", Jordan Journal of Mechanical and Industrial Engineering,Vol. 11, No. Specialissue, 2017, pp. 235–243.

[25] Air Movement and Control Association. Fans and systems. Illinois: West University Drive Arlington Heights, 2011.

[26] M. Maine, M. El Oumami, O. Bouksour, and B. Nassiri, "Study of the effect of some deflector's geometry factors on the reduction of the aerodynamic drag of the car model", Jordan Journal of Mechanical and Industrial Engineering, Vol. 15, No. 3, 2021, pp. 265–272.

[27] T. K. Sahoo and P. Ghose, "Effect of Inlet Swirl on Combustion Performance and Soot Formation of a Turbulent Methane-Air Non-Premixed Flame", Jordan Journal of Mechanical and Industrial Engineering, Vol. 16, No. 2, 2022, pp. 309–318.

[28] Y. Taamneh, "CFD simulations of drag and separation flow around ellipsoids",Jordan Journal of Mechanical and Industrial Engineering, Vol. 5, No. 2, 2011, pp. 129–132.

[29] "Case fan 80x80x20 mm for 12 VDC for computer and chassis with ball bearing 2X - Cablematic." https://cablematic.com/en/products/case-fan-80x80x20-mm-for-12-vdc-for-computer-and-chassis-with-ball-bearing-2x-VL068/#extra_product_info (accessed Dec. 24, 2023).

[30] D. C. Axial, F. Dc, R. Fans, D. C. Fans, and O. Dc, "DC Fans DC Fans", [Online]. Available: chrome-extension://efaidnbmnnnibpcajpcglclefindmkaj/https://www.mouser.com/datasheet/2/433/DC_FANS_Wakefield_Vette_Data_Sheet_rev_A-1710305.pdf

[31] "NF-A8 FLX || Specifications." https://noctua.at/en/products/fan/nf-a8-flx/specification (accessed Dec. 24, 2023).

[32] "8020 Cpu Fan Specifications 80x80x20mm Dc Cooling 5v 12v 24v 80mm Dc Fan - Buy 8020 Cpu Fan Specifications,80x80x20mm Dc Cooling Fan,5v 12v 24v 80mm Dc Fan Product on Alibaba.com." https://www.alibaba.com/product-detail/8020-cpu-fan-specifications-80x80x20mm-dc_60812074606.html (accessed Dec. 24, 2023).

[33] "Noise Prediction - 2018 - What's New in SOLIDWORKS." https://help.solidworks.com/2018/english/WhatsNew/c_noise_prediction.htm (accessed Jan. 16, 2024).

[34] A. Hossain, A. Rahman, J. Hossen, P. Iqbal, N. Shaari, and G. K. Sivaraj, "Drag reduction in a wing model using a bird feather like winglet", Jordan Journal of Mechanical and Industrial Engineering, Vol. 5, No. 3, 2011, pp. 267–272.

[35] H. Moria, H. Chowdhury, F. Alam, and A. Subic, "Aero/hydrodynamic Study of Speedo LZR, TYR Sayonara and Blueseventy Pointzero3 swimsuits",Jordan Journal of Mechanical and Industrial Engineering, Vol. 5, No. 1, 2011, pp. 83–88.